Analysis of a Thick Dichroic Plate with Arbitrarily Shaped Holes

W. A. Imbriale[1]

A thick dichroic plate acts as a frequency selective surface (FSS) in that it is transparent at one frequency while at the same time reflective to other frequencies. It is used in the DSN to enable simultaneous multiple-frequency operation. Most of the plates currently in use were designed with programs that analyzed only the simple geometries, such as circular or rectangular holes. Since it is too expensive to experimentally determine the FSS parameters, only designs that could be accurately analyzed were chosen, and it is the primary reason why the recent FSS designs use rectangular holes. To achieve the sharp corners of the rectangular holes, it was necessary to use an electrical discharge machining (EDM) manufacturing technique. This manufacturing technique is expensive, and an important use of the arbitrary-shaped analysis is to enable designs that use rounded corners that are able to be manufactured by less expensive techniques.

The analysis is accomplished by combining the finite-element method (FEM) for determining the waveguide modes of arbitrarily shaped guides with the method of moments and Floquet mode theory for periodic structures. The software was verified by comparison with previously measured and computed dichroic plates.

I. Introduction

The ability to transmit and receive simultaneously at multiple frequency bands is an important requirement for the DSN. This is usually accomplished either by using a dual-band feed or by using separate feeds and a frequency-selective surface (FSS), typically referred to as a dichroic plate.

The first use of a dichroic plate was as part of the reflex-dichroic feed system used on the 64-meter antenna [1]. This first dichroic plate consisted of circular holes in a half-wavelength-thick metallic plate. All subsequent dichroic plates used in the DSN were also thick plates with holes. The discussion that follows treats the most general case of the analysis of a thick dichroic plate with arbitrarily shaped holes at arbitrary angles of incidence. However, most of the plates currently in use in the DSN were designed with programs that analyzed only the simple geometries, such as circular [2] or rectangular [3] holes. This analysis limitation also impacted the choice of FSS designs. Since it is too expensive to experimentally determine the FSS parameters, only designs that could be accurately analyzed were chosen, and this is

[1] Communications Ground Systems Section.

The research described in this publication was carried out by the Jet Propulsion Laboratory, California Institute of Technology, under a contract with the National Aeronautics and Space Administration.

the primary reason why the recent FSS designs use rectangular holes. To achieve the sharp corners of the rectangular holes, it was necessary to use an electrical discharge machining (EDM) manufacturing technique. This manufacturing technique is expensive, and an important use of the arbitrarily shaped analysis is to enable designs that use rounded corners that are able to be manufactured by less expensive techniques.

The analysis parallels the development for the rectangular-hole case except that the waveguide modes are generated using the finite-element method instead of using the closed-form expressions available for the rectangular waveguide.

The relationship between the holes, the array lattice of an infinite dichroic plate, and the incident wave is shown in Fig. 1. The design variables are the hole size and shape, lattice size and shape, thickness of the plate, dielectric constant in the hole, and angle of incidence of the linearly polarized wave. The program calculates the amplitude and phase of both the transmission and reflection coefficients of the two orthogonal linear polarizations—the transverse electric (TE) and transverse magnetic (TM).

The analysis of a thick dichroic plate with arbitrarily shaped holes is carried out in a series of steps very similar to the technique described in [3]. First, a model of a half-space infinite array is constructed. A complete set of basis functions with unknown coefficients is developed for the waveguide region (waveguide modes) and for the free-space region (Floquet modes) [4] in order to represent the electromagnetic fields. Next the boundary conditions are applied at the interface between these two regions. The method of moments is used to compute the unknown mode coefficients [2,5]. The scattering matrix of the half-space infinite array is then calculated. The reference plane of the scattering matrix is moved half-a-plate thickness in the negative z-direction. Finally, a dichroic plate of finite thickness is synthesized by positioning two plates of half thickness back to back. The total scattering matrix is obtained by cascading the scattering matrices of the two half-space infinite arrays.

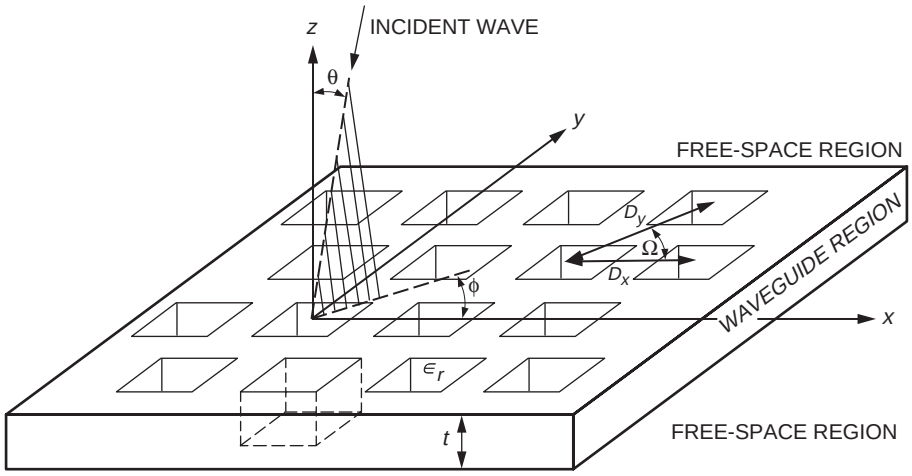

Fig. 1. Geometry of a thick dichroic plate with holes.

II. Finite-Element Formulation of the Waveguide Problem

The analysis starts with an infinite array in half space (Fig. 2) consisting of a free-space region ($z < 0$) and a waveguide region ($z > 0$). The electromagnetic fields in each region are represented by a set of orthonormal basis functions, Floquet and waveguide modes, respectively, that satisfy Maxwell's equations.

The finite-element method is used to compute the waveguide modes. The development is given in several references, including [6], but will be repeated here for completeness and notational conformance.

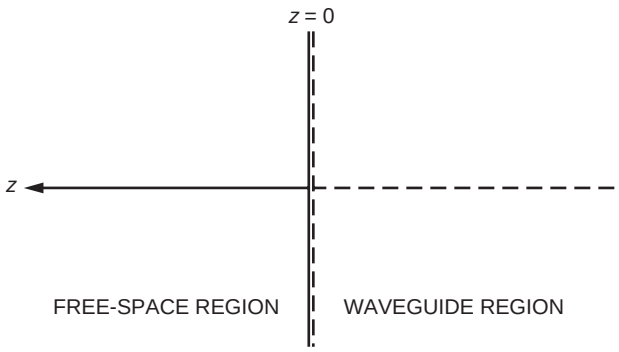

Fig. 2. Half-space infinite array with reference at *z* = 0.

As is well known, the propagating mode of a hollow, uniform waveguide may be determined by solving the two-dimensional scalar Helmholtz equation,

$$\left(\nabla^2 + k^2\right) \Psi = 0 \tag{1}$$

Here Ψ represents the magnitude of an axially directed electric or magnetic Hertz vector. If the transverse electric (TE) modes of the guide are desired, Ψ is the electric Hertz vector, and must satisfy the homogeneous Neumann boundary condition

$$\frac{\partial \Psi}{\partial n} = 0 \tag{2}$$

while the transverse magnetic (TM) modes are obtained if Ψ is taken to be the magnetic Hertz vector, subject to the boundary condition

$$\Psi = 0 \tag{3}$$

everywhere along the guide walls.

Rather than attempting to solve this eigenvalue problem directly, the finite-element method reframes it in variational terms. It is shown in books on mathematical physics [7] that the solution of the Helmholtz equation with homogeneous boundary conditions is equivalent to minimizing the functional $\mathcal{F}$ defined by

$$\mathcal{F} = \iint_R \left(- \left|\mathrm{grad}\varphi\right|^2 + k^2\varphi^2 \right) dxdy \tag{4}$$

The region of integration is, of course, the waveguide cross-section. If a trial solution $\varphi(x, y)$ is represented geometrically as a surface spanning the region R over the x–y plane, the correct surface $\Psi(x, y)$ is that which yields the smallest possible value of $\mathcal{F}$.

In the finite-element method, the correct solution will be approximated by a surface $\varphi(x, y)$ made up of finite surface elements of a simple kind. For simplicity, all the elementary regions are taken to be triangles. Corresponding to each elementary region, a surface element will be defined by requiring $\varphi(x, y)$ to be a linear function of its values at the vertices; thus φ is then defined by

$$\varphi(x,y) = \sum_{i=1}^{N} \alpha_i(x,y)\varphi_i \tag{5}$$

$\mathcal{F}$ is now an ordinary function of the parameters that define φ, in this case the vertex values φ_i:

$$\mathcal{F}(\varphi) = F\left(\varphi_1, \varphi_2, \cdots, \varphi_N\right) \tag{6}$$

The solution is found by minimizing F with respect to all the parameters. That is, it will be required that

$$\frac{\partial F}{\partial \varphi_m} = 0 \tag{7}$$

for all m. If the region R contains altogether N vertices, this minimization requirement changes Eq. (4) into a matrix eigenvalue problem of order N, as will be shown next.

A. The Matrix Eigenvalue Problem

In view of Eq. (6), the minimization requirement, Eq. (7), is equivalent to

$$\iint_R \frac{\partial}{\partial \varphi_m} \left|\text{grad}\varphi\right|^2 dxdy = k^2 \iint_R \frac{\partial}{\partial \varphi_m}\varphi^2 dxdy \tag{8}$$

Differentiating repeatedly, one finds from Eq. (5) that

$$\frac{\partial}{\partial \varphi_m} \left|\text{grad}\varphi\right|^2 = 2\sum_{k=1}^{N} \left(\frac{\partial \alpha_m}{\partial x}\frac{\partial \alpha_k}{\partial x} + \frac{\partial \alpha_m}{\partial y}\frac{\partial \alpha_k}{\partial y} \right) \varphi_k \tag{9}$$

everywhere within an elementary region that abuts on vertex m. Elsewhere, α_m is zero, so that the right-hand side vanishes. By carrying out a similar differentiation, one next finds that

$$\frac{\partial}{\partial \varphi_m}\left(\varphi^2\right) = 2\sum_{k=1}^{N} \alpha_m \alpha_k \varphi_k \tag{10}$$

where again nonzero terms arise on the right-hand side only if both vertices m and k are vertices of the triangle in question.

It will be convenient to define the purely geometric quantities

$$S_{mk} = \iint_R \left(\frac{\partial \alpha_m}{\partial x}\frac{\partial \alpha_k}{\partial x} + \frac{\partial \alpha_m}{\partial y}\frac{\partial \alpha_k}{\partial y} \right) dxdy \tag{11}$$

and

$$T_{mk} = \iint_R \alpha_m \alpha_k dxdy \tag{12}$$

which express the nature of the region R and the manner of its subdivision into elementary regions. In terms of these integral quantities, Eq. (8) reads

$$S\Phi = k^2 T\Phi \tag{13}$$

where Φ is the column matrix of vertex values φ_i, and S and T are square matrices of order N, whose elements are S_{mk} and T_{mk}, as defined above. Minimization of $\mathcal{F}$ is thus equivalent to the eigenvalue problem, Eq. (13), and solution of the latter will provide approximate eigenvalues and eigenfunctions for the boundary-value problem. It will be noted that S and T are always symmetric, and the eigenvalues therefore always real.

B. Matrices *S* and *T* for Triangle Elements

If linear triangular elements are used, the unknown function ϕ within each element is approximated as

$$\phi^e(x, y) = a^e + b^e x + c^e y \tag{14}$$

where a^e, b^e, and c^e are constant coefficients to be determined and e is the element number. For a linear triangular element, there are three nodes located at the vertices of the triangle (Fig. 3). Assume that the nodes are numbered counterclockwise by numerals 1, 2, and 3, with the corresponding values of ϕ denoted by ϕ_1^e, ϕ_2^e, and ϕ_3^e, respectively. Enforcing Eq. (14) at the three nodes, we obtain

$$\phi_1^e = a^e + b^e x_1^e + c^e y_1^e$$

$$\phi_2^e = a^e + b^e x_2^e + c^e y_2^e$$

$$\phi_3^e = a^e + b^e x_3^e + c^e y_3^e$$

Solving for the constant coefficients a^e, b^e, and c^e in terms of ϕ_1^e, and substituting them back into Eq. (14) yields

$$\phi^e(x, y) = \sum_{j=1}^{3} N_j^e(x, y)\phi_j^e \tag{15}$$

where $N_j^e(x, y)$ is the interpolation or expansion functions given by

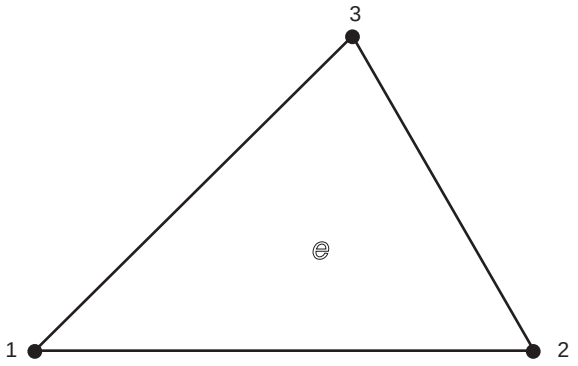

Fig. 3. Linear triangular element.

$$N_j^e(x,y) = \frac{1}{2A}\left(a_j^e + b_j^e x + c_j^e y\right), \quad j = 1,2,3 \tag{16}$$

in which

$$\left.\begin{array}{lll} a_1^e = x_2^e y_3^e - y_2^e x_3^e; & b_1^e = y_2^e - y_3^e; & c_1^e = x_3^e - x_2^e \\ a_2^e = x_3^e y_1^e - y_3^e x_1^e; & b_2^e = y_3^e - y_1^e; & c_2^e = x_1^e - x_3^e \\ a_3^e = x_1^e y_2^e - y_1^e x_2^e; & b_3^e = y_1^e - y_2^e; & c_3^e = x_2^e - x_1^e \end{array}\right\} \tag{17}$$

and

$$A = \frac{1}{2}\begin{vmatrix} 1 & x_1^e & y_1^e \\ 1 & x_2^e & y_2^e \\ 1 & x_3^e & y_3^e \end{vmatrix} = \frac{1}{2}\left(b_1^e c_2^e - b_2^e c_1^e\right)$$

$$= \text{area of the } e\text{th element} \tag{18}$$

In the above, x_j^e and $y_j^e (j = 1,2,3)$ denote the coordinate values of the jth node in the eth element. It can be easily shown that the interpolation functions have the property

$$N_i^e\left(x_j^e, y_j^e\right) = \delta_{ij} = \begin{cases} 1 & i = j \\ 0 & i \neq j \end{cases} \tag{19}$$

and, as a result, at node i, ϕ^e in Eq. (15) reduces to its nodal value, ϕ_i^e.

For ease in both analysis and computer programming, it is useful to regard the matrices S and T as being composed of sums of sparse matrices of order N, typically $s^{(i)}$ and $t^{(i)}$, made up of the contributions to the S and T matrices that are attributable to only one elementary region, say the ith. That is to say, one may write

$$S_{mk} = \sum_i s_{mk}^{(i)} \tag{20}$$

$$T_{mk} = \sum_i t_{mk}^{(i)} \tag{21}$$

Clearly, $s_{mk}^{(i)} = t_{mk}^{(i)} = 0$ whenever n equals neither m nor k, i.e., for all elements that touch neither vertex m nor k. Explicit expressions for the element matrix components are

$$s_{mk}^{(i)} = \int_i \int \left(\frac{\partial \alpha_m}{\partial x}\frac{\partial \alpha_k}{\partial x} + \frac{\partial \alpha_m}{\partial y}\frac{\partial \alpha_k}{\partial y}\right) dxdy \tag{22}$$

$$t_{mk}^{(i)} = \int_i \int \alpha_m \alpha_k dxdy \tag{23}$$

the integrations being carried out over the ith elementary region. For triangular elementary regions, $s^{(i)}$ and $t^{(i)}$ in general possess nine nonzero components and are symmetric. These component values are found by substituting Eq. (15) into Eq. (22):

$$s_{mk}^{(i)} = \frac{1}{4A^2} \int_i \int (b_m b_k + c_m c_k)\, dxdy \tag{24}$$

On carrying out the necessary integration,

$$s_{mk}^{(i)} = \frac{-1}{4A} \left[(x_m^e - x_i^e)(x_k^e - x_i^e) + (y_m^e - y_i^e)(y_k^e - y_i^e) \right] \tag{25}$$

Similarly, substitution into Eq. (23) yields the surprisingly simple result

$$t_{mk}^{(i)} = \begin{cases} \dfrac{1}{12} A, & m \neq k \\ \dfrac{1}{6} A, & m = k \end{cases} \tag{26}$$

Leaving out all rows and columns composed of zeros only, a single triangular element is thus described by the matrix contributions

$$\begin{bmatrix} s_{11} & s_{12} & s_{13} \\ s_{21} & s_{22} & s_{23} \\ s_{31} & s_{32} & s_{33} \end{bmatrix} \begin{bmatrix} \varphi_1 \\ \varphi_2 \\ \varphi_3 \end{bmatrix} = k^2 \frac{A}{12} \begin{bmatrix} 2 & 1 & 1 \\ 1 & 2 & 1 \\ 1 & 1 & 2 \end{bmatrix} \begin{bmatrix} \varphi_1 \\ \varphi_2 \\ \varphi_3 \end{bmatrix} \tag{27}$$

where the s_{mk} are calculated from Eq. (25), and the area A is given by Eq. (18).

III. Boundary Conditions and Method of Moments

The electromagnetic field in the waveguide is expressed as a sum of incident and reflected waveguide modes, while in the free-space region it is expressed as a sum of incident and reflected Floquet modes. Boundary conditions are applied at the interface between two regions, i.e., the transverse electric and magnetic fields must be continuous across the junction at $z = 0$. This leads to an integral equation for the unknown transverse electric field at the boundary. The infinite-array scattering problem then becomes similar to a two-region waveguide problem.

The method of moments is used to transform the integral equation into a matrix equation suitable for evaluation on a digital computer. Solving the set of linear equations gives the unknown mode coefficients in both regions.

A. Integral Equation Formulation

In the waveguide region, the total transverse electric field and magnetic field (see Fig. 2) at $z = 0^+$ is given by

$$\left.\begin{aligned} E_T^w(x,y) &= \sum_{i=1}^{\infty} \bar{e}_i^w(x,y)\Big(a_i^w + b_i^w\Big) \\ H_T^w(x,y) &= \sum_{i=1}^{\infty} y_i\, \hat{z} \times e_i^w(x,y)\Big(a_i^w - b_i^w\Big) \end{aligned}\right\} \tag{28}$$

where $\bar{e}_i^w(x,y)$ represents the modal fields in the waveguide and, for TE modes,

$$\left.\begin{aligned} \bar{e}_i^w(x,y) &= \hat{z} \times \nabla\Psi^{TE} \\ y_{TE} &= \frac{\gamma_i}{j\omega\mu} \end{aligned}\right\} \tag{29}$$

and, for TM modes,

$$\left.\begin{aligned} \bar{e}_i^w(x,y) &= -\nabla\Psi^{TM} \\ y_{TM} &= \frac{j\omega\varepsilon}{\gamma_i} \end{aligned}\right\} \tag{30}$$

with Ψ^{TE} and Ψ^{TM} given by the finite-element method (FEM) solution of the waveguide.

It should be noted that Ψ and $\nabla\Psi$ are real functions and the Ψ vectors are normalized so that

$$\int_{wg} \nabla\Psi_i \nabla\Psi_j ds = \int_{wg} \bar{e}_i \cdot \bar{e}_j ds = \delta_{ij} \tag{31}$$

Forming the inner product of the ith waveguide mode with the total transverse electric field, Eq. (28), we obtain an expression for the unknown modal coefficients,

$$\iint_{wg} \bar{e}_i^w \cdot E_T^w dxdy = a_i^w + b_i^w \tag{32}$$

Note that it is also possible to extend the integral over the entire Floquet cell since $\bar{E}_T = 0$ outside the waveguide. Using Eq. (32) in the $\bar{H}_T$ field expression, it is possible to write

$$H_T = 2\sum_{i=1}^{\infty} y_i a_i^w\, (\hat{z} \times \bar{e}_i^w) - \sum_{i=1}^{\infty} y_i\, (\hat{z} \times \bar{e}_i^w) \iint_{wg} e_i^w \times E_T^w dx'dy' \tag{33}$$

In a very similar manner, the total electric and magnetic fields at $z = 0^-$ are given by

$$\left.\begin{aligned} E_T^-(x,y) &= \sum_{j=1}^{\infty} \bar{e}_j^F \left(a_j^F + b_j^F\right) \\ H_T^-(x,y) &= -\sum_{j=1}^{\infty} Y_j \left(\hat{z} \times \bar{e}_j^F\right)\left(a_j^F - b_j^F\right) \end{aligned}\right\} \tag{34}$$

where, for TE modes,

$$\left.\begin{aligned} \bar{e}_j^F &= \hat{z} \times \nabla \phi_i^{TE} \\ Y_{TE} &= \frac{\gamma_i}{j\omega\mu} \end{aligned}\right\} \tag{35}$$

and, for TM modes,

$$\left.\begin{aligned} \bar{e}_j^F &= -\nabla \phi_i^{TM} \\ Y_{TM} &= \frac{j\omega\varepsilon}{\gamma_i} \end{aligned}\right\} \tag{36}$$

However, ϕ_j and $\nabla\phi_j$ are complex functions that are normalized so that

$$\int\limits_{\substack{\text{Floquet} \\ \text{cell}}} \nabla\phi_i \cdot \nabla\phi_j^* ds = \int \bar{e}_i \cdot \bar{e}_j^* ds = \delta_{ij} \tag{37}$$

The Floquet modes on the skewed grid (skew angle Ω) and grid spacing D_x, D_y (Fig. 1) are given by [4]

$$\phi_{mn} = \frac{e^{j(\alpha_m x + \beta_n y)}}{\sqrt{D_x D_y \sin\Omega}\sqrt{\alpha_m^2 + \beta_n^2}} \tag{38}$$

for either TE or TM waves (same boundary conditions!):

$$\alpha_m = \frac{2\pi m}{D_x} - k_0 \sin\theta\cos\phi \tag{39}$$

and

$$\beta_n = \frac{2\pi n}{D_y \sin\Omega} - \frac{2\pi m}{D_x}\cot\Omega - k_0 \sin\theta\sin\phi \tag{40}$$

where k_0 is the wave number in free space.

In much the same way as with the waveguide modes, we can show

$$\iint_A e_j^* \cdot \bar{E}_T^- dx'dy' = a_j^F + b_j^F \tag{41}$$

$$H_T^- = -2\sum_{j=1}^{\infty} a_j^F \left(\hat{z} \times \bar{e}_j^F\right) Y_j + \sum_{j=1}^{\infty} Y_j \left(\bar{z} \times \bar{e}_j^F\right) \iint_A e_j^* \cdot E_T^- dx'dy' \tag{42}$$

The transverse electric and magnetic fields must be continuous across the junction at $z = 0$. Thus, equating the magnetic fields yields

$$2\sum_{i=1}^{\infty} y_i a_i^w \bar{e}_i^w + 2\sum_{j=1}^{\infty} a_j^F Y_j e_j^F = \sum_{j=1}^{\infty} y_i \bar{e}_i^w \iint_A \bar{e}_i^w \cdot E_T\left(x', y'\right) dx'dy'$$

$$+ \sum_{j=1}^{\infty} Y_j \bar{e}_j^F \iint_A \bar{e}_j^{F^*} \cdot E_T\left(x', y'\right) dx'dy' \tag{43}$$

B. Moment Method Solution

To solve the integral equation, it is necessary to expand the unknown electric field in terms of a set of basis functions. The obvious choice for this is the waveguide modes $\bar{e}_k^w(x, y)$. Thus,

$$\bar{E}_T\left(x', y'\right) = \sum_{k=1}^{\infty} c_k \bar{e}_k^w\left(x', y'\right) \tag{44}$$

Substituting this expression into the integral equation and interchanging the order of summation and integration yields

$$2\sum_{i=1}^{\infty} y_i a_i^w \bar{e}_i^w + 2\sum_{j=1}^{\infty} a_j^F Y_j \bar{e}_j^F = \sum_{k=1}^{\infty}\sum_{i=1}^{\infty} c_k y_i \bar{e}_i^w + \sum_{k=1}^{\infty}\sum_{i=1}^{\infty} c_k Y_j \bar{e}_j^F \iint_A e_j^F \cdot \bar{e}_k^w dx'dy' \tag{45}$$

To simplify the notation, define the inner product known as the intermodal coupling coefficient:

$$I_{kj} = \iint \bar{e}_k^w\left(x', y'\right) \cdot \bar{e}_j^F\left(x', y'\right) dx'dy' \tag{46}$$

Using this notation, the equation simplifies to

$$2\sum_{i=1}^{\infty} y_i a_i^w e_i^w + 2\sum_{j=1}^{\infty} a_j^F Y_j e_j^F = \sum_k c_k \left[\sum_i y_i e_i^w + \sum_j Y_j e_j^F I_{ky}\right] \tag{47}$$

To apply the moment method, we must take the inner product with the weighting. In this analysis, we use the same basis functions (Galerkin). Thus, multiply Eq. (47) by $e_\ell^w(x, y)$ and integrate over the waveguide. This yields the matrix equation

$$2\sum_i a_i^w y_i + 2\sum_j a_j^F Y_j I_{ej} = \sum_k \left[\sum_i y_i + \sum_j Y_j I_{\ell j} I_{kj}\right] c_k \tag{48}$$

Using the following definitions,

$$M_{\ell k} = \sum_i y_i + \sum_j Y_j I_{\ell j} I_{kj} \tag{49}$$

and

$$G_\ell = 2\sum_i a_i^w y_i + 2\sum_j a_j^F Y_j I_{\ell j} \tag{50}$$

Thus, Eq. (48) can be expressed as

$$G_\ell = \sum_k M_{\ell k} C_k \tag{51a}$$

or

$$[G] = [M]\,[C] \tag{51b}$$

The solution for the unknown mode coefficients is then given by

$$[C] = [M]^{-1}\,[G] \tag{52}$$

Generally, the scattered fields are the primary quantities of interest and can be derived from the mode coefficients. Recalling

$$b_i^w = \iint e_i^w \cdot E_T^w dxdy - a_i^w \tag{53}$$

then

$$\left.\begin{aligned} b_i^w &= \iint e_i^w \cdot \sum_k c_K e_k^w dxdy - a_i^w \\ b_i^w &= c_i - a_i^w \end{aligned}\right\} \tag{54}$$

Similarly,

$$b_j^F = \sum_k c_k I_{kj} - a_j^F \tag{55}$$

IV. Scattering Matrix and Reference Plane

The characteristics of the infinite array referenced to $z = 0$ are represented by a scattering matrix S that contains the transmission and reflection information for the free-space/waveguide junction:

$$S = \begin{bmatrix} S_{11} & S_{12} \\ S_{21} & S_{22} \end{bmatrix} \tag{56}$$

where S_{11}, S_{12}, S_{21}, and S_{22} are matrices with 1 representing the free-space region and 2 the waveguide region. The size of matrix S_{11} is 2 by 2; S_{22} is n by n; S_{12} is 2 by n; S_{21} is n by 2; and n is the number of waveguide modes used. For an arbitrary set of incident waveguide modes contained in vector a_1 and incident TE_{00} and TM_{00} Floquet modes contained in vector a_2, the reflected mode vectors b_1 and b_2 are determined by the following set of equations:

$$\left.\begin{aligned} b_1 &= S_{11}a_1 + S_{12}a_2 \\ b_2 &= S_{21}a_1 + S_{22}a_2 \end{aligned}\right\} \tag{57}$$

Moving the reference plane in the waveguide region from $z = 0$ to $z = -t/2$ (Fig. 4), where t is the thickness of the plate, the elements of the new scattering matrix S' become

$$S'_{11}(u,v) = S_{11}(u,v) \tag{58}$$

$$S'_{12}(u,v) = S_{12}(u,v)\exp\left(-j\gamma_v\frac{t}{2}\right) \tag{59}$$

$$S'_{21}(u,v) = S_{21}(u,v)\exp\left(-j\gamma_u\frac{t}{2}\right) \tag{60}$$

$$S'_{22}(u,v) = S_{22}(u,v)\exp\left[\left(-j\gamma_u\frac{t}{2}\right)\left(-j\gamma_v\frac{t}{2}\right)\right] \tag{61}$$

where γ_u and γ_v are the propagation constants of modes u and v.

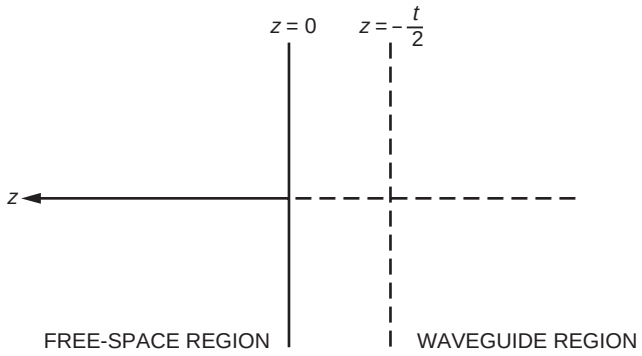

Fig. 4. Half-space infinite array with reference at $z = -t/2$.

V. Cascading the Finite Thickness

Scattering by a dichroic plate with finite thickness can be analyzed by considering two infinite-array problems. The space is divided into four regions: a free-space region (region I), two waveguide regions (regions II and III), and another free-space region (region IV), as shown in Fig. 5. The scattering matrix with reference to $z = -t/2$ for regions I and II is S', and the scattering matrix with reference to $z = -t/2$ for regions III and IV isS'', which is the transpose matrix of S':

$$S''_{11} = S'_{22} \tag{62}$$

$$S''_{12} = S'_{21} \tag{63}$$

$$S''_{21} = S'_{12} \tag{64}$$

$$S''_{22} = S'_{11} \tag{65}$$

The scattering matrix S^T for the finite-thickness plate is determined by cascading these two matrices:

$$S^T_{11} = S'_{12} \left(I - S''_{11} S'_{22}\right)^{-1} S''_{11} S'_{21} + S'_{11} \tag{66}$$

$$S^T_{12} = S'_{12} \left(I - S''_{11} S'_{22}\right)^{-1} S''_{12} \tag{67}$$

$$S^T_{21} = S'_{21} \left(I - S''_{22} S'_{11}\right)^{-1} S''_{21} \tag{68}$$

$$S^T_{22} = S''_{21} \left(I - S'_{22} S''_{11}\right)^{-1} S'_{22} S''_{12} + S''_{22} \tag{69}$$

where I is a unitary matrix.

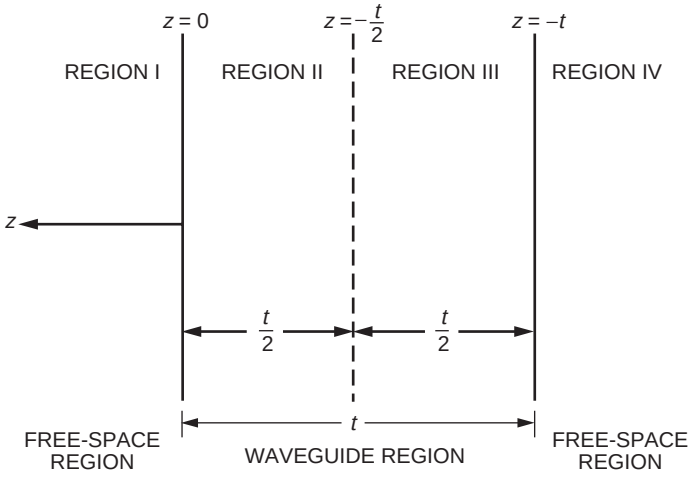

Fig. 5. The finite-thickness (t) plate is analyzed by considering two infinite-array problems.

VI. Computing the Intermodal Coupling Coefficients

The intermodal coupling coefficients are given as

$$I_{kj} = \iint_A \bar{e}_k^w (x', y') \cdot \bar{e}_j^F (x', y') \, dx' dy' \tag{70}$$

Using Eq. (38),

$$\phi_{mn} = \frac{e^{j(\alpha_m x + \beta_n y)}}{\sqrt{D_x D_y \sin \Omega} \sqrt{\alpha_m^2 + \beta_m^2}}$$

then, for TE modes,

$$\bar{e}_i^F = \hat{z} \times \nabla \phi_{mn} \tag{71}$$

and, for TM modes,

$$\bar{e}_i^F = -\nabla \phi_{mn} \tag{72}$$

where i represents the mn mode.

Also, for the waveguide modes, let

$$\Psi_i^{\mathrm{TE,TM}} = \sum_{t=1}^{NT} \sum_{j=1}^{3} N_{jt}(x, y) \phi_{jt}^{\mathrm{TE,TM}} \tag{73}$$

where $\phi_{jt}^{\mathrm{TM,TE}}$ is the solution for the ith mode of the finite-element waveguide eigenmode problem described in Section II. Also, recall that, for TE modes,

$$e_i^\omega = \hat{z} \times \nabla \Psi_i^{\mathrm{TE}} \tag{74}$$

and, for TM modes,

$$e_i^\omega = -\nabla \Psi_i^{\mathrm{TM}} \tag{75}$$

There are then four expressions for the intermodal coupling coefficients formed by combining TE and TM waveguide modes with TE and TM Floquet modes.

To develop the expression for the TE waveguide, TE Floquet mode, substitute the expressions for $\bar{e}_i^F$ and $\bar{e}_i^\omega$ into Eq. (70) and integrate. Defining

$$S_e(\alpha, \beta) = \int_{i\text{th triangle}} e^{j(\alpha x + \beta y)} dx dy$$

which is the Fourier transform of the triangular shape function for the ith triangle of the finite-element grid (see [8] for the closed-form expression to evaluate the integral), then we can write for the TE waveguide, TE Floquet mode

$$I_{kj} = -\sum_{e=1}^{NT}\sum_{i=1}^{3} \frac{\left(c_i^e \phi_i^e \beta_j + b_i^e \phi_i^e \alpha_j\right)\ {}^* S_e}{\left(\sqrt{\alpha_j^2 + \beta_j^2}\right)\left(\sqrt{D_x D_y \sin\Omega}\, 2A_e\right)}$$

where c_i^e and b_i^e are given by Eq. (17) for each triangle, and the ϕ_i^{ek} are the values for the kth eigenmode on the eth triangle. There are very similar-looking expressions for the other TE,TM combinations.

VII. The Frequency-Selective Surface Finite-Element (FSSFE) Computer Program

There are a number of steps required to compute the reflection and transmission coefficients of arbitrarily shaped holes in a thick plate:

(1) The hole is defined by a sequence of x, y boundary points. There are also various subroutines that generate the required set of boundary points for specific shapes, i.e., rectangular, cross-shaped, circular, Pyle, etc.

(2) The next step is to generate the finite-element grid. This is done using a Delaunay triangularization with a public domain computer program, delaundo, based on a Ph.D. thesis by Jans-Dominik Müller [9]. Delaundo creates triangular grids based on the frontal Delaunay method (Frod) [10]. First the set of discretized curves that describes the boundary is triangulated. This initial mesh is suitable for interpolation of a local mesh size throughout the domain after a few modifications in the connections are made by the algorithm. New internal vertices are then created on frontal edges between well-shaped and ill-shaped triangles such that a new triangle with the desired size and a good shape will result.

Thus, the algorithm is similar to the various Delaunay methods in that the resulting triangulation observes a circum-circle criterion. It is also akin to advancing front methods in that new vertices are introduced in layers on the boundaries in a very regular fashion. The regularity of the point distribution and, thus, the element quality are enhanced by an averaging process that tends to choose an equilibrium position between competing edges when the front is refined or coarsened.

(3) After the grid has been generated, the finite-element method of Section II is utilized to generate the waveguide eigenvectors and eigenvalues. The S and T matrices are filled, and the corresponding eigenvalue problem is solved using ARPACK [11], a collection of FORTRAN77 subroutines designed to solve large-scale eigenvalue problems. ARPACK is designed to compute a few eigenvalues and corresponding eigenvectors of a general n-by-n matrix A. It is most appropriate for large sparse or structured matrices A, where structured means that a matrix–vector product $w \leq Av$ requires order n rather than the usual order $n^{**}2$ floating-point operations. This software is based upon an algorithmic variant of the Arnoldi process called the implicitly restarted Arnoldi method (IRAM). When the matrix A is symmetric, it reduces to a variant of the Lanczos process called the implicitly restarted Lanczos method (IRLM). These variants may be viewed as a synthesis of the Arnoldi/Lanczos process with the implicitly shifted QR algorithm that is suitable for large-scale problems. For many standard problems, a matrix factorization is not required. Only the action of the matrix on a vector is needed. However, for the generalized case that exists for the finite-element problem $Sx = k^2 Tx$, it is necessary to factor the matrix T. Since T is sparse, the sparse matrix solver given in [12] is used.

(4) The solution then proceeds as shown in Sections III through VI. The intermodal coupling coefficients are computed and the matrix M is formed and inverted. Next the terms of the scattering matrix for the free-space/waveguide junction are computed. The scattering matrices are then shifted and cascaded to compute the scattering coefficients for the finite-thickness plate.

VIII. Verification of the Computer Code

The first test of the arbitrarily shaped hole computer code was to see if it could duplicate the results from the earlier code [3] that could only do rectangular-shaped holes. The case analyzed is the same test dichroic plate fabricated to verify the rectangular-hole computer code. The dimensions of the plate are $H_x = 1.850$ cm, $H_y = 1.923$ cm, $D_x = 2.388$ cm, $D_y = 2.388$ cm, and $\Omega = 60.0$ deg. And, $t = 3.584$ cm, with a tolerance of 0.0025 cm. Figure 6 plots the TE and TM reflection coefficients for the two codes and demonstrates that the new code accurately computes the reflection coefficients of the rectangular geometry. Satisfactory convergence is achieved by using 40 waveguide modes and gridding the hole with 1683 triangles. Figures 7 and 8, reproduced from [3], show that the analysis also agrees with the measured data.

The first dichroic plate used in the DSN is described in [1] and consisted of an array of hexagonally packed 2.237-cm-diameter holes drilled normal to the plate surfaces. The plate is 3.576-cm thick, and the center-to-center hole spacing is 2.388 cm. It was designed using the Chen Holey Plate computer program [2], and the computer program shows that the plate E- and H-plane resonant frequencies (30-deg incident wave tilt from normal) are 8.481 and 8.363 GHz, respectively. The FSSFE program gives 8.497 and 8.350 GHz, respectively. The small difference is probably because the Chen program does not use a sufficient number of waveguide modes. At the operational frequency, a differential phase shift of 11.3 deg (11.6 deg with the FSSFE program) and an ellipticity of 1.75 dB was predicted. This dichroic plate depolarization was cured by making the holes slightly non-circular in cross section, thus introducing a different E- and H-plane phase shift to counteract the 11.3-deg phase shift. The particular hole cross section selected was "Pyle guide" [13]. The dichroic design was approximate in that the design procedure was to adjust the guide geometry (using a program developed by Knud Pontoppidan for computing

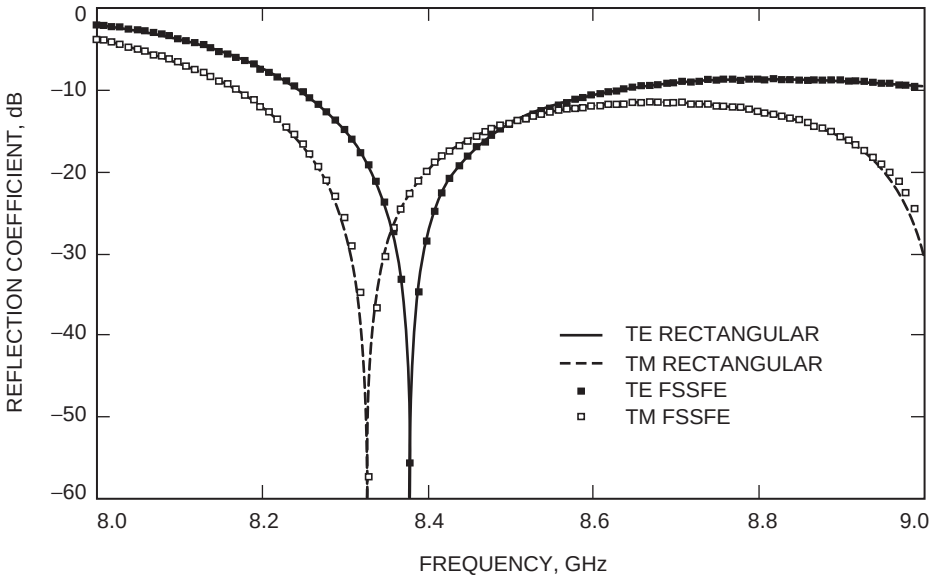

Fig. 6. Rectangular versus FSSFE code.

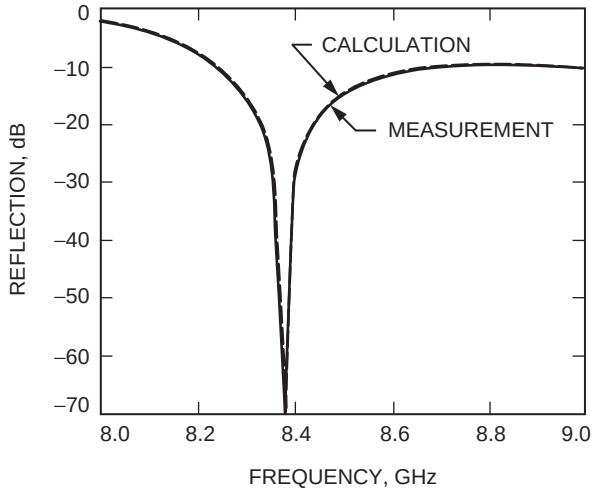

Fig. 7. Measured and calculated reflection versus frequency for the test dichroic plate for TE polarization.

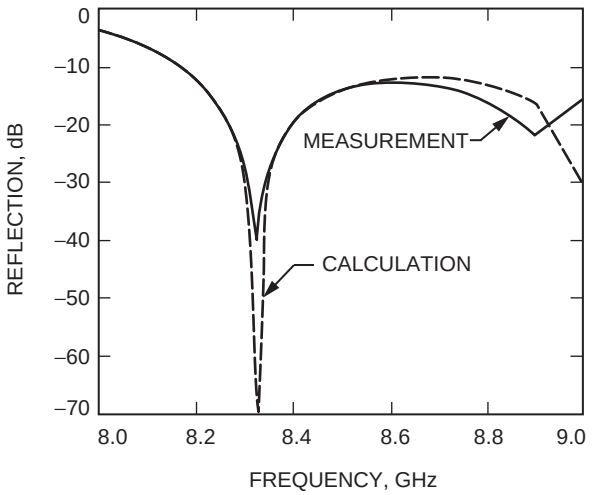

Fig. 8. Measured and calculated reflection versus frequency for the test dichroic plate for TM polarization.

the guide wavelength numbers [14]) until the plate electrical thickness at 8.415 GHz corresponded to those in the original circular-hole plate at 8.481 and 8.363 GHz, respectively. There was no FSS program at that time that could compute the reflection and transmission coefficients for the actual Pyle plate. A comparison of a measured Pyle plate [15] and the FSSFE program is shown in Fig. 9. For reference, a gridding of the guide is shown in Fig. 10.

Another plate built for the DSN that was only approximately analyzed was the cross-shaped plate [16] designed to pass both the transmit (7.145–7.235 GHz) and receive (8.4–8.5 GHz) X-band frequencies while reflecting the S-band frequencies (2.090–2.320 GHz). The analytic technique used to design the plate was to assume infinitely thin walls and then to build a plate with as thin a wall as possible. The FSSFE program can analyze the exact cross geometry, including the thickness of the walls. A plot of the measured data versus frequency compared to the calculated data from FSSFE is shown in Fig. 11, demonstrating the accuracy of the FSSFE program. The hole geometry is shown in Fig. 12, and the plate was 3.167-cm thick.

IX. Conclusions

A computer code that can accurately compute the reflection and transmission coefficients from a thick dichroic plate with arbitrarily shaped holes has been described. The code was verified by comparisons both to earlier but more restrictive computer programs (circular and rectangular holes) and to measured data for plates built with rectangular, Pyle, and cross-shaped holes.

Both the rectangular-hole and cross-shaped-hole plates were manufactured using a very accurate but very expensive electrical discharge machining (EDM) process. The EDM process produces very accurate holes with sharp (square) corners. With the new analysis tool, it is now possible to design dichroics with rounded corners that may be manufactured by a less expensive water jet or machining process. Work is currently under way to design and fabricate dichroic plates using the less expensive manufacturing processes and will be the subject of a follow-on article.

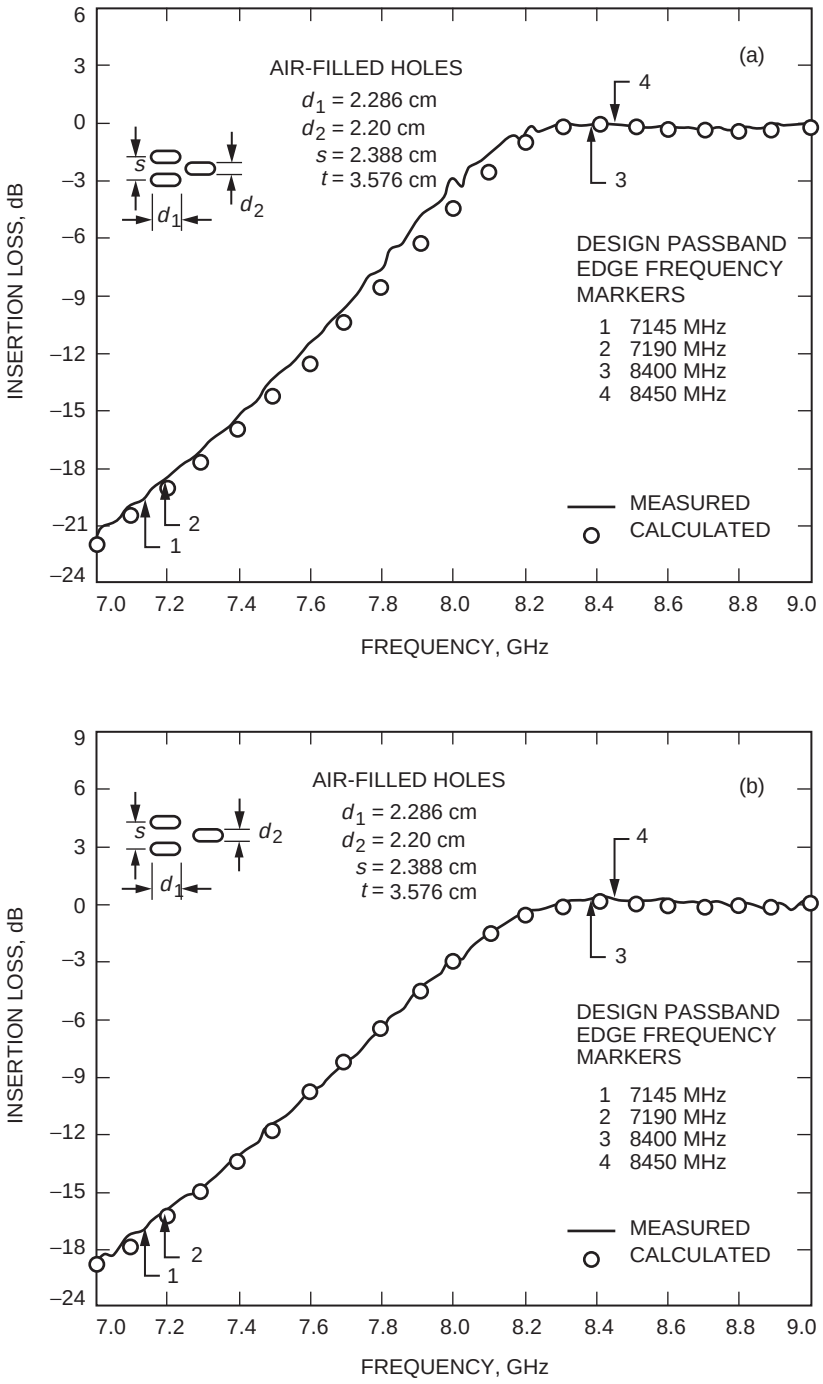

Fig. 9. Measured and calculated transmission loss versus frequency for DSN Pyle plate: (a) TE polarization and (b) TM polarization.

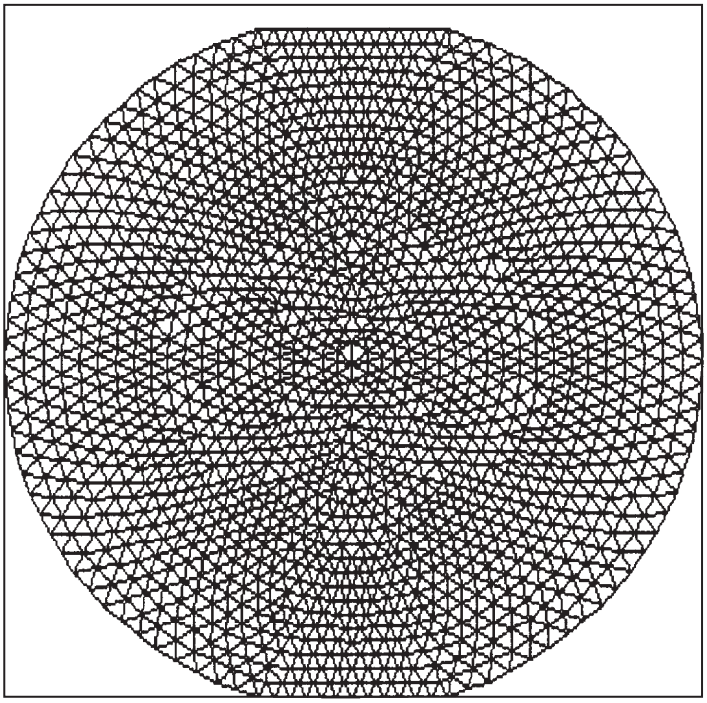

Fig. 10. Finite-element gridding for a Pyle plate.

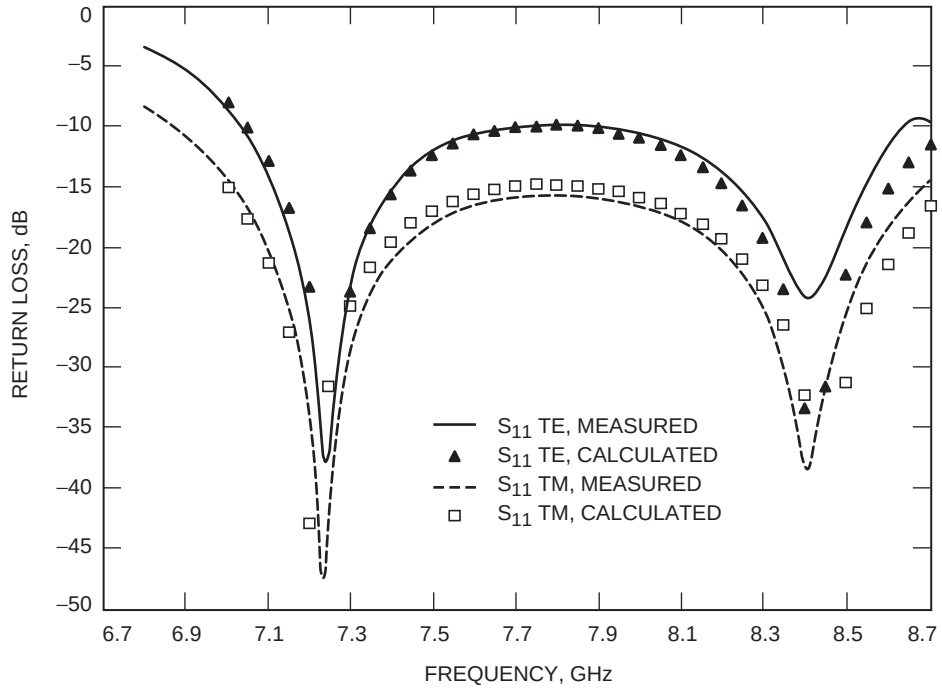

Fig. 11. Measured and calculated reflection coefficient for cross-shaped plate.

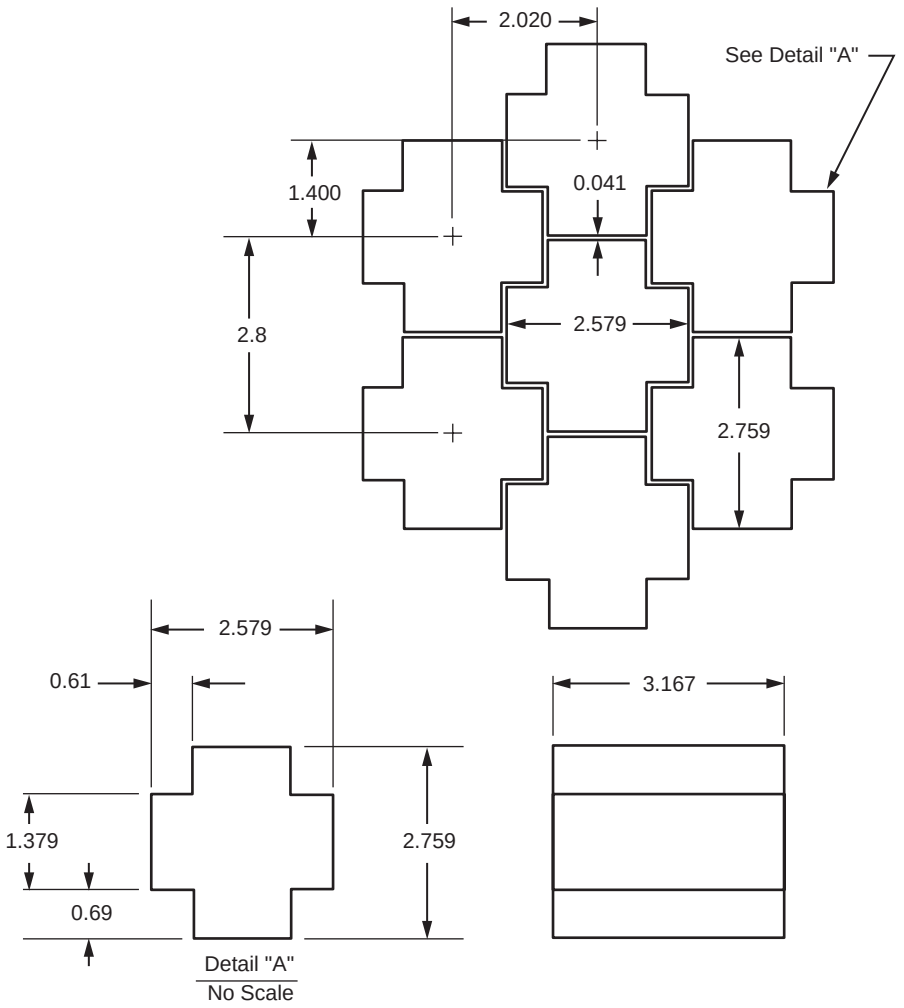

Fig. 12. Cross-shaped plate geometry (all units in cm).

Acknowledgments

As it is with many scientific/engineering endeavors, this work is built upon the shoulders of many other people. I want to thank Dan Hoppe for his many helpful technical discussions, as Dan had developed a similar program for Hughes. A significant amount of code was used from the rectangular-hole program of Jackie Chen. Glen Welsh and Dan Hoppe modified the delaundo code to make it useful for meshing waveguides. Tom Cwik supplied the code that was used to factor and solve the sparse matrix.

References

[1] P. D. Potter, "S- and X-Band Feed System," *The Deep Space Network Progress Report 32-1526*, vol. XV, Jet Propulsion Laboratory, Pasadena, California, pp. 54–62, June 15, 1973.
http://tmo.jpl.nasa.gov/tmo/progress_report/XV/XVI.PDF

[2] C. C. Chen, "Transmission of Microwave Through Perforated Flat Plates of Finite Thickness," *IEEE Transactions on Microwave Theory and Techniques*, vol. MTT-21, no. 1, pp. 1–6, January 1973.

[3] J. C. Chen, "Analysis of a Thick Dichroic Plate with Rectangular Holes at Arbitrary Angles of Incidence," *The Telecommunications and Data Acquisition Progress Report 42-104, October–December 1990*, Jet Propulsion Laboratory, Pasadena, California, pp. 9–16, February 15, 1991.
http://tmo.jpl.nasa.gov/tmo/progress_report/42-104/104B.PDF

[4] N. Amitay, V. Galindo, and C. P. Wu, *Theory and Analysis of Phased Array Antennas*, New York: Wiley-Interscience, 1972.

[5] C. C. Chen, "Transmission Through a Conducting Screen Perforated Periodically with Apertures," *IEEE Trans. Microwave Theory Tech.*, vol. MTT-18, no. 9, pp. 627–632, September 1970.

[6] R. Silvester, "Finite-Element Solution of Homogeneous Waveguide Problems," *Alta Frequenza*, vol. 38, pp. 313–317, 1969.

[7] P. M. Morse and H. Fishbach, *Methods of Theoretical Physics (Part I)*, New York: Macmillan, 1968.

[8] W. A. Imbriale and R. E. Hodges, "The Linear Phase Triangular Facet Approximation in Physical Optics Analysis of Reflector Antennas," *Applied Computational Electromagnetic Society*, vol. 6, no. 2, pp. 74–85, Winter 1991.

[9] J.-D. Müller, *On Triangles and Flow*, Ph.D. Thesis, The University of Michigan, Ann Arbor, 1996.

[10] J.-D. Müller, "The Advancing Front Method and the Delaunay Triangulation," 24th von Karman Institute Lecture Series on Computational Fluid Dynamics, vol. 2, 1994.

[11] R. Lehoucq, K. Maschhoff, D. Sorensen, and C. Yang, ARPACK SOFTWARE.
http://www.caam.rice.edu/software/ARPACK/

[12] T. Cwik, D. S. Katz, and J. Patterson, "Scalable Solutions to Integral-Equation and Finite-Element Simulations," Advanced Numerical Techniques in Electromagnetics, *IEEE Trans. Antennas Propagation*, vol. 45, pp. 544–555, 1997.

[13] J. R. Pyle, "Cutoff Wavelengths of Waveguides with Unusual Cross Sections," *IEEE Transactions on Microwave Theory and Techniques*, Correspondence, vol. MTT-12, no. 5, pp. 556–557, September 1964.

[14] K. Pontoppidan, "Finite-Element Techniques Applied to Waveguides of Arbitrary Cross Sections, Parts I and II," Ph.D. Thesis, The Technical University of Denmark, Lyngby, Denmark, September 1971.

[15] T. Y. Otoshi and M. M. Franco, "Dual Passband Dichroic Plate for X-Band," *The Telecommunications and Data Acquisition Progress Report 42-94, April–June 1988*, Jet Propulsion Laboratory, Pasadena, California, pp. 110–134, August 15, 1988.
http://tmo.jpl.nasa.gov/tmo/progress_report/42-94/94J.PDF

[16] L. W. Epp, P. H. Stanton, R. E. Jorgenson, and R. Mittra, "Experimental Verification of an Integral Equation Solution for a Thin-Walled Dichroic Plate with Cross-shaped Holes," *T-AP*, vol. 42, no. 6, pp. 878–882, June 1994.